A Hybrid Inductive Power Transfer System With Misalignment Tolerance Using Quadruple-D Quadrature Pads

Yang Chen, *Student Member, IEEE*, Bin Yang, Xiaobing Zhou, Qiao Li, Zhengyou He, *Senior Member, IEEE*, Ruikun Mai, *Member, IEEE*, and Jih-Sheng Lai, *Life Fellow, IEEE*

***Abstract*—Pad misalignments are almost inevitable in most inductive power transfer (IPT) systems. It tends to cause parameter variations and, thus, significantly affects the performance of the IPT system. In this article, a hybrid IPT system with misalignment tolerance using the quadruple-D quadrature pads (QDQPs) is proposed to tolerate the *x*, *y*, *z*, and diagonal misalignments with load-independent output voltage, simplifying or even canceling control schemes. Besides, the proposed approach can restrict the increase of the primary current when the secondary side moves out of the operating region. Moreover, a new parametric design method is presented according to the misalignment characteristics of QDQPs. The method can limit the output voltage fluctuation to a certain range, given a predetermined misalignment distance. A 3.5-kW prototype was built to verify the proposed hybrid IPT system. The primary and secondary coil sizes are 400 mm × 400 mm, and the air gap is 150 mm. Experimental results demonstrate that the proposed hybrid system can tolerate −150 to +150 mm *x*-misalignment, −150 to +150 mm *y*-misalignment, −20 to +35 mm *z*-misalignment, and −100 to +100 mm diagonal misalignment with load-independent output voltage. Within the predetermined misalignment range, the output voltage fluctuation is less than 5%.**

***Index Terms*—Hybrid topology, inductive power transfer (IPT), misalignment tolerance, quadruple-D quadrature pads (QDQPs).**

I. Introduction

INDUCTIVE power transfer (IPT) technology has been employed in numerous applications, such as consumer electronics [1], biomedical implant devices [2], underwater power supplies [3], and electric vehicles (EVs) [4], [5]. IPT systems have advantages of safety, convenience, and flexibility over the traditional conductive power supply systems because the energy is delivered from power sources to loads through magnetic coupling without the physical contact.

In IPT charging applications, misalignment tolerance is always one of the biggest concerns. Pad misalignments generally include the lateral (*x*), longitudinal (*y*), and vertical (*z*) misalignments between the primary and secondary coils. Misalignments are almost inevitable and can cause parameter variations, especially mutual inductance, resulting in the reduction of power transfer capability, high power losses, and instability. Therefore, it is crucial to mitigate the above-mentioned problem. Moreover, if an IPT system can not only tolerate pads misalignments but also operate under the load-independent condition, the control scheme of the system can be simplified dramatically.

A. Related Works

Many works have been done on how to improve the misalignment tolerance for IPT systems. Generally speaking, these approaches can be roughly classified into four categories.

1) Control Schemes: It is straightforward that applying a dc–dc converter [6], [7] on the primary or the secondary sides can regulate the output current/voltage of the IPT system against the displacement of the pad. The phase shift control [8] can also modulate the output current/voltage with pad misalignments. In another aspect, the robust control [9] is introduced to improve the output performance responding to the coil misalignments. These methods control the output power flow by regulating the duty cycle, which has to be changed in a wide range with large couplings or load variations. The converter may suffer from an extensive input modulation index and complicated control circuitry. In [10], the frequency tuning approach is proposed to keep the output power stable versus the variable coupling coefficient by adjusting the frequency of the primary side to compensate the variations of the mutual inductance. This method changes the operating frequency in a roomy sphere, and the load is fixed, so the application is limited. Usually, most of the controllers need an RF communication increasing the extra cost. The speed and accuracy of controllers and communication might lead to reliability problems [11]. The following three scenarios improving tolerance to misalignments can simplify the control schemes.

Manuscript received April 22, 2019; revised August 15, 2019 and October 6, 2019; accepted November 18, 2019. Date of publication November 20, 2019; date of current version February 20, 2020. This work was supported in part by the National Key Research and Development Program of China under Grant 2017YFB1201002, in part by the National Natural Science Foundation of China under Grants 51977184 and 51677155, in part by the Applied Basic Research Programs of Science and Technology Commission Foundation of Sichuan Province under Grant 2018JY0586, in part by the State Scholarship Fund of China Scholarship Council under Grant 201807000025, and in part by the Cultivation Program for the Excellent Doctoral Dissertation of Southwest Jiaotong University under Grant 2016310066. Recommended for publication by Associate Editor S. C. Tan. *(Corresponding author: Ruikun Mai.)*

Y. Chen, B. Yang, X. Zhou, Q. Li, Z. He, and R. Mai are with the School of Electrical Engineering, Southwest Jiaotong University, Chengdu 611756, China (e-mail: yang.chen92@foxmail.com; 546867343@qq.com; 1030027934@qq.com; 574143439@qq.com; hezy@home.swjtu.edu.cn; mairk@swjtu.edu.cn).

J.-S. Lai is with Future Energy Electronics Center, Virginia Polytechnic Institute and State University, Blacksburg, VA 24061 USA (e-mail: laijs@vt.edu).

Color versions of one or more of the figures in this article are available online at http://ieeexplore.ieee.org.

Digital Object Identifier 10.1109/TPEL.2019.2954906

2) Magnetic Coupler Design: As for the magnetic coupler design, Choi *et al*. [12] and Elliott *et al*. [13] introduce asymmetric coils and multiphase pickups for lateral tolerance IPT systems. A number of primary coils are placed in adjacency to build the uniform magnetic field for the battery charging platform [14], [15]. Besides, double-D, bipolar, and tripolar magnetic couplers are proposed in [16]–[18] to provide uniform magnetic field distribution. In [19], Zheng *et al.* propose the asymmetric magnetic coupling to increase the tolerance for the displacement. These methods [14]–[19] can guarantee the misalignments of pickups in the *x*- and *y*-directions. For three-dimensional (3-D) aspect, two kinds of magnetic pads are proposed in [20] and [21] to receive power at an arbitrary angle in 3-D space. All these approaches are mainly to shape the magnetic flux to relatively uniform for the pickups.

3) Topology Parameter Optimization: The parameter design of compensation topology is another type of method to improve the misalignment performance for IPT systems. In [22], Zhu *et al*. propose a method to optimize the compensation capacitors of a four-coil coupled IPT system, and the tolerant misalignment is improved to 44.3% of the coil size with the output fluctuation of more than 15%. A reformed inductor–capacitor–capacitor (*LCC*) compensated topology is utilized to realize robust reaction to displacement [23]. The output power drop is less than 20% when the coupling coefficient increases to twice the nominal value. In [24], Lu *et al*. introduce a dual-coupled *LCC*-compensated network to enlarge the misalignment tolerance. It can maintain at least 56.8% and 82.6% of well-aligned power with 33.3% displacement in the *x*- and *y*-directions. In [25], a general design method for a T-type compensation topology is proposed to retain the constant output power. A dual-side detuned series–series (SS) compensation topology is presented in [26]. The power fluctuation is less than 20% with coupling coefficient variation from 0.08 to 0.2. However, these methods as mentioned above cannot allow IPT systems operating load independently.

4) Hybrid Topology: Hybrid topologies combining two different compensation topologies with complementary characteristics can improve misalignment tolerance. Villa *et al*. [27] use series–parallel–series hybrid topology (the combination of SS and PS topologies) to transfer the rated power with 25% lateral misalignment. Besides, a hybrid IPT system integrating the SS and *LCC–LCC* topologies can maintain 95% of nominal power with 17% vertical and 41% longitudinal misalignments [28]. In [29], Chen *et al*. put forward another hybrid (combination of S-*LCC* and *LCC*-S topologies) IPT system, which can tolerate 50% *y*-misalignment and 33.3% *z*-misalignment charging batteries with 5% change rate of output current/voltage. However, in [28] and [29], when the secondary side moves far away from the primary side, the current in S compensation topology increases exponentially and even destroys the system. The *x*-misalignments of the two hybrid systems are relatively smaller comparing with that of the *y*-direction.

B. Contributions

The main contributions of this article are summarized as follows.

1) This article proposes a hybrid IPT system with misalignment tolerance. The hybrid system consists of *LCC*-S and S-*LCC* compensation topologies. The primary *LCC* and S topologies connect in series while the secondary S and *LCC* topologies connect in parallel. The proposed approach can restrict the primary inverter current to increase dramatically when the secondary side moves out of the operating region. Besides, the hybrid IPT system can tolerate misalignment in the *x*, *y*, *z*, and diagonal directions, and the output voltage is load independent.
2) Quadruple-D quadrature pads (QDQPs) are used in the hybrid IPT system. The misalignment characteristics of the QDQPs are elaborated in this article. Then, an innovative parametric design method is proposed to limit the output voltage fluctuation to a certain range within a predetermined misalignment distance, simplifying the control schemes.

The rest of the article is organized as follows. In Section II, the hybrid IPT system is systematically analyzed. Section III presents the displacement characteristics of the QDQPs and analyzes the parametric design method in detail. Experimental results are provided in Section IV to validate the proposed method. Finally, Section V concludes this article.

II. Theoretical Analysis

The proposed hybrid IPT topology is illustrated in Fig. 1, where the high-frequency inverter and full-bridge rectifier are formed with four MOSFETs ($Q_1 - Q_4$) and four diodes ($D_1 - D_4$), respectively. L_1, C_1, $C_{\rm P1}$, and $C_{\rm S1}$ constitute the *LCC*-S compensation topology, while the S-*LCC* compensation network comprises $C_{\rm P2}$, L_2, C_2, and $C_{\rm S2}$. The primary *LCC* and S topologies are connected in series, while the secondary S and *LCC* network are connected in parallel. $V_{\rm in}$ and $V_{\rm o}$ are the input and output dc voltages. The mutual inductances between the four coils are, respectively, $M_{\rm P1S1}$, $M_{\rm P1S2}$, $M_{\rm P1P2}$, $M_{\rm P2S1}$, $M_{\rm P2S2}$, and M_{S1S2}. In practice, inductor L_1 and capacitor $C_{\rm P2}$ can be regarded as one passive component inductor L_e or capacitor C_e, of which the relationship is given by

$$\begin{cases} L_e = L_1 - 1/\left(\omega^2 C_{\rm P2}\right), & \text{if } \omega L_1 - 1/\left(\omega C_{\rm P2}\right) > 0 \\ C_e = C_{\rm P2}/\left(1 - \omega^2 L_1 C_{\rm P2}\right), & \text{if } \omega L_1 - 1/\left(\omega C_{\rm P2}\right) < 0. \end{cases} \tag{1}$$

$R_{\rm CD}$ is the equivalent ac load of the rectifier, and the equation of $R_{\rm CD}$ and dc load R is expressed by [30]

$$R_{\rm CD} = \frac{8}{\pi^2} R. \tag{2}$$

The power losses of the resonant tanks are ignored for simplification. The fundamental harmonics approximation method is utilized to analyze the system. Then, the hybrid compensation topology is regarded as being driven by a sinusoidal voltage source with angular frequency ω because of the high-quality factors of the resonant tanks. The resonant tanks satisfy the following equations, i.e.,

$$\begin{cases} \omega^2 L_1 C_1 = \omega^2 L_2 C_2 = \omega^2 L_{\rm S1} C_{\rm S1} = \omega^2 L_{\rm P2} C_{\rm P2} = 1 \\ \omega^2 \left(L_{\rm P1} - L_1\right) C_{\rm P1} = \omega^2 \left(L_{\rm S2} - L_2\right) C_{\rm S2} = 1. \end{cases} \tag{3}$$

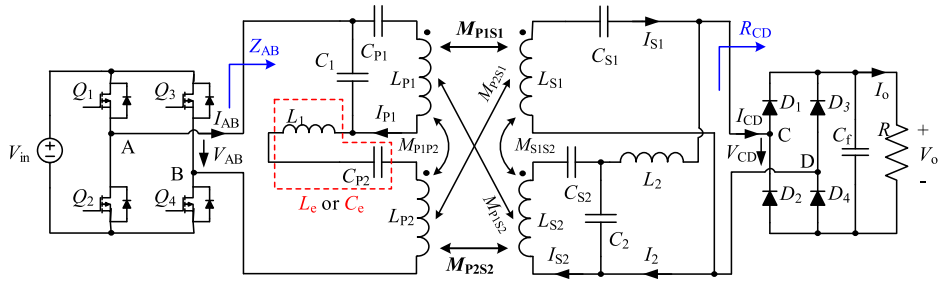

Fig. 1. Proposed hybrid IPT topology.

According to Kirchhoff's laws, the circuit can be described by

$$\begin{bmatrix} V_{AB} \\ 0 \\ 0 \\ 0 \\ 0 \end{bmatrix} = \begin{bmatrix} Z_{11} & Z_{12} & Z_{13} & Z_{14} & Z_{15} \\ Z_{21} & Z_{22} & Z_{23} & Z_{24} & Z_{25} \\ Z_{31} & Z_{32} & Z_{33} & Z_{34} & Z_{35} \\ Z_{41} & Z_{42} & Z_{43} & Z_{44} & Z_{45} \\ Z_{51} & Z_{52} & Z_{53} & Z_{54} & Z_{55} \end{bmatrix} \begin{bmatrix} I_{AB} \\ I_{P1} \\ I_{S1} \\ I_{S2} \\ I_{CD} \end{bmatrix} \tag{4}$$

where $Z_{11} = 0$, $Z_{12} = Z_{21} = -1/(j\omega C_1)$, $Z_{13} = Z_{31} = -j\omega M_{P2S1}$, $Z_{14} = Z_{41} = -j\omega M_{P2S2}$, $Z_{15} = Z_{51} = 0$, $Z_{22} = 0$, $Z_{23} = Z_{32} = -j\omega M_{P1S1}$, $Z_{24} = Z_{42} = -j\omega M_{P1S2}$, $Z_{25} = Z_{52} = 0$, $Z_{33} = R_{CD}$, $Z_{34} = Z_{43} = 0$, $Z_{35} = Z_{53} = R_{CD}$, $Z_{44} = 0$, $Z_{45} = Z_{54} = -1/(j\omega C_1)$, and $Z_{55} = R_{CD}$.

Only the main couplings (M_{P1S1} and M_{P2S2}) are taken into consideration, while the effects of the cross couplings (M_{P1S2}, M_{P1P2}, M_{P2S1}, and M_{S1S2}) on the output can be neglected with properly designed magnetic pads, which will be discussed in Section III. Thus, after solving (4), the currents can be yielded as

$$\begin{cases} I_{AB} = \dfrac{V_{AB} M_{P1S1}^2 L_2^2}{R_{ac}(M_{P1S1}M_{P2S2}+L_1L_2)^2}, \; I_{P1} = \dfrac{-jV_{AB}L_2}{\omega(M_{P1S1}M_{P2S2}+L_1L_2)} \\ I_{S1} = \dfrac{V_{AB} M_{P1S1} L_1 L_2^2}{R_{ac}(M_{P1S1}M_{P2S2}+L_1L_2)^2}, \; I_{S2} = \dfrac{jV_{AB}M_{P1S1}}{\omega(M_{P1S1}M_{P2S2}+L_1L_2)} \\ I_2 = \dfrac{V_{AB} M_{P1S1}^2 M_{P2S2} L_2}{R_{ac}(M_{P1S1}M_{P2S2}+L_1L_2)^2}. \end{cases} \tag{5}$$

Then, the input equivalent impedance Z_{AB} can be deduced as

$$Z_{AB} = \frac{V_{AB}}{I_{AB}} = \frac{R_{ac}(M_{P1S1}M_{P2S2} + L_1L_2)^2}{M_{P1S1}^2 L_2^2} \tag{6}$$

which is pure resistant demonstrating that the output current and voltage of the inverter can achieve zero-phase angle (ZPA).

For the primary currents I_{AB} and I_{P1}, when the secondary side is far away from the primary side, the main mutual inductances approach zero, so we have $\lim_{M_{P1S1}\to 0,\, M_{P2S2}\to 0} I_{AB} = 0$ and $\lim_{M_{P1S1}\to 0,\, M_{P2S2}\to 0} I_{P1} = -jV_{AB}/(\omega L_1)$. Namely, the primary currents will not increase exponentially when the pickup moves out of the operating region, eliminating the drawback of the primary S compensation topology.

The voltage gain G_{VV} of the hybrid topology is derived by

$$G_{VV} = \frac{V_{CD}}{V_{AB}} = \frac{R_{CD}\,(I_{S1} + I_2)}{V_{AB}} = \left(\frac{M_{P2S2}}{L_2} + \frac{L_1}{M_{P1S1}}\right)^{-1}. \tag{7}$$

Equation (7) indicates that the output current is load independent without considering the effects of the cross couplings. Besides, the main mutual inductances (M_{P1S1} and M_{P2S2}) will decrease (or increase) with misalignment. So, the value of M_{P2S2}/L_2 will decrease (or increase) while the value of L_1/M_{P1S1} will increase (or decrease). As a result, given the properly designed parameters, the sum of M_{P2S2}/L_2 and L_1/M_{P1S1} can remain relatively constant within a predetermined misalignment distance. Hereinafter, the sum of M_{P2S2}/L_2 and L_1/M_{P1S1} is defined as the equivalent gain coefficient (EGC) in this article, i.e., EGC $= M_{P2S2}/L_2 + L_1/M_{P1S1}$.

III. Parametric Design of the Hybrid System

A. Misalignment Analysis of QDQPs

According to the theoretical analysis in Section II, the magnetic coupler should satisfy the following requirements.

1) Our coils are required to form the magnetic coupler, i.e., two transmitters and two receivers.
2) With the *x*-, *y*-, or *z*-misalignment, only two main couplings (M_{P1S1} and M_{P2S2}) work, and the cross couplings (M_{P1S2}, M_{P1P2}, M_{P2S1}, and M_{S1S2}) should be small enough to be neglected.

Quadruple D pad (QDP) is reported in [31] and [32] for the laptop and EV charging applications. In this article, a quadrature pad (QP) is added to the QDP to form the QDQP, as shown in Fig. 2. The size of each D coil of the QDP is the same, and the primary and secondary QDQPs are symmetrical. Ferrite cores (PC40) are placed close to the QDQPs to increase the coupling. The shape of the QDQP is set as a square, so the *x*- and *y*-misalignment performances are the same. As mentioned in Section II, only the main couplings (M_{P1S1} and M_{P2S2}) are considered, and the cross couplings should be designed to zero or small enough. Thus, the direction of the current in the adjacent coils of QDP should be the opposite, so the QDP and QP can be decoupled. Take the primary coils, L_{P1} and L_{P2}, as examples. The two coils are in the center of the magnetic coupler in different layers. The magnetic flux excited by the QDP L_{P2} is symmetrical in space, and the amount of the magnetic flux flows into the QP L_{P1} equals that flows out of it. Therefore, the magnetic flux ψ_{P2P1} passing through L_{P1} is zero, and the coupling mutual inductance M_{P2P1} is very small, even close to zero, as shown

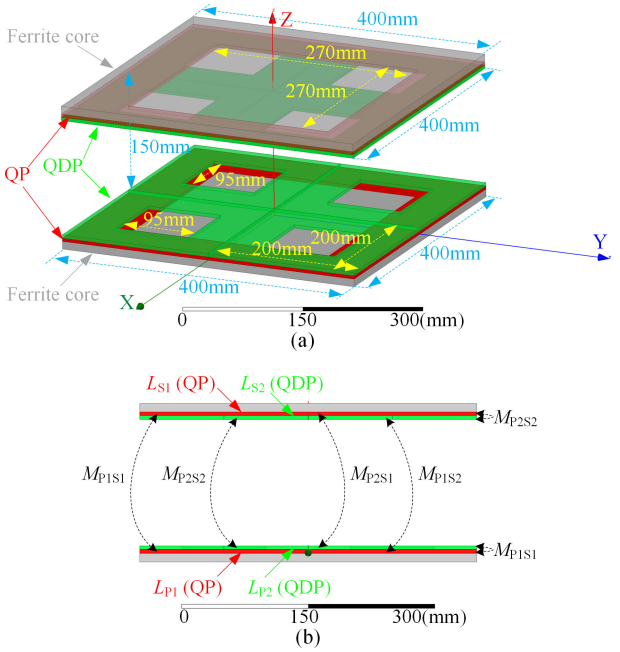

Fig. 2. Structure of the proposed QDQPs. (a) Coil size. (b) Mutual inductances.

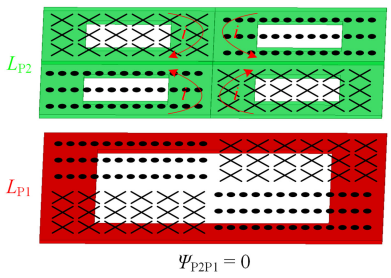

Fig. 3. Magnetic flux excited by L_{P2} passes through the coil L_{P1}.

in Fig. 3. Similarly, we can figure out that other cross couplings are also very small, even near to zero.

Since the QDQP is symmetric about the *x*- and *y*-axis, the misalignment performances are the same in the *x* and *y* directions. Thus, the *x*- and *z*-misalignments are principally discussed in this article. The mutual inductances of the QDQPs with misalignment in the *x*- and *z*-directions are measured, as drawn in Fig. 4(a) and (b). It is obvious that the main mutual inductances (M_{P1S1} and M_{P2S2}) have large variations with misalignments, while the cross couplings (M_{P1S2}, M_{P1P2}, M_{P2S1}, and M_{S1S2}) are so small that they can be ignored. Moreover, the variation trends of M_{P1S1} and M_{P2S2} are nearly the same, which indicates that the relationship between the two mutual inductances might be expressed by a function [29]. Likely, the *xy* (diagonal) misalignment curve is given in Fig. 4(c). The main mutual inductances (M_{P1S1} and M_{P2S2}) have large variations with misalignment, while the primary/secondary cross couplings (M_{P1P2} and M_{S1S2}) are so small that they can be ignored. The primary and secondary cross couplings (M_{P1S2} and M_{P2S1}) cannot be neglected once the diagonal misalignment is larger than 100 mm, which can degrade the misalignment performance.

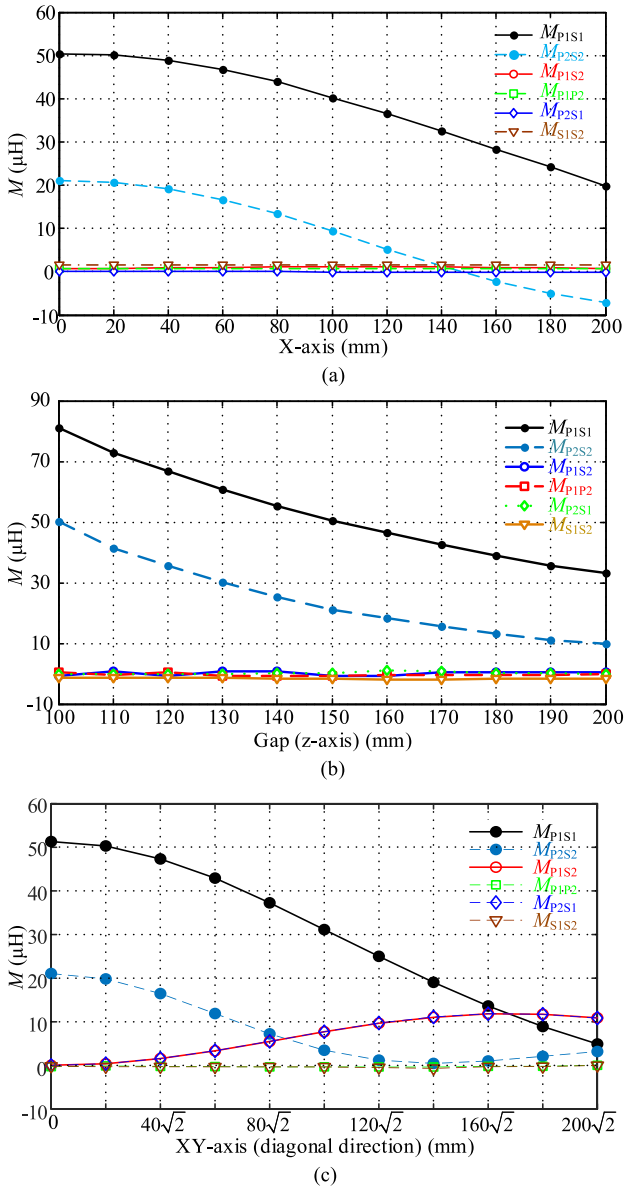

Fig. 4. Variations of mutual inductances due to the misalignment in the (a) *x*-, (b) *z*-, and (c) *xy*-direction (i.e., diagonal direction).

B. Parametric Design Method

In accordance with the analysis in Section II, selecting the proper parameters of the hybrid IPT system, EGC can maintain relatively constant. Namely, the variation of the output voltage can be limited to a certain range. In this article, the output voltage variation δ_V is defined as [34]

$$\delta_V = \frac{V_{o\text{-}max} - V_{o-min}}{V_{o-max} + V_{o-min}} \times 100\% \tag{8}$$

where V_{o-max} and V_{o-min} are the maximum and minimum output voltages of the IPT system within a predetermined misalignment distance.

The parameters are designed in a well-aligned case, i.e., the nominal operating point (NOP) (0, 0, 150) of the hybrid IPT system. In this circumstance, the nominal voltage gain and the nominal mutual inductance between L_{P1} and L_{S1} are marked as G_{VVN} and M_{P1S1N}.

The output voltage of the inverter is a square wave, and V_{AB} is expressed as (9) through the Fourier decomposition

$$V_{\mathrm{AB}} = \frac{2\sqrt{2}V_{\mathrm{in}}}{\pi}. \tag{9}$$

Similarly, the relationship between the input and output voltages of the rectifier is given by

$$V_{\mathrm{o}} = \frac{\pi\sqrt{2}V_{\mathrm{CD}}}{4}. \tag{10}$$

Afterward, the nominal voltage gain G_{VVN} turns out to be

$$G_{\mathrm{VVN}} = \frac{V_{\mathrm{CD}}}{V_{\mathrm{AB}}} = \frac{V_{\mathrm{o}}}{V_{\mathrm{in}}}. \tag{11}$$

According to the misalignment curves, the relationship between the two main mutual inductances can approximately be expressed as a linear function within a certain misalignment range, namely

$$M_{\mathrm{P2S2}}\left(M_{\mathrm{P1S1}}\right) = aM_{\mathrm{P1S1}} + b \tag{12}$$

where a and b are the coefficients of the linear function, which can be calculated with the help of MATLAB using a polynomial curve fitting function. It should be noticed that if the misalignment curves are changed, the parameters a and b should be redesigned accordingly.

Then, substituting (12) into (7), the voltage gain is rewritten as

$$G_{\mathrm{VV}}\left(M_{\mathrm{P1S1}}\right) = \left(\frac{aM_{\mathrm{P1S1}} + b}{L_2} + \frac{L_1}{M_{\mathrm{P1S1}}}\right)^{-1}. \tag{13}$$

In Fig. 5, M_{P1S1min} and M_{P1S1max} are the minimum and maximum mutual inductances within the determined misalignment range. G_{VVmin} and G_{VVmax} are the minimum and maximum voltage gains, respectively

$$\begin{cases} G_{\mathrm{VVmax}} = \left(1 + \delta_{\mathrm{V}}\right) G_{\mathrm{VVN}} \\ G_{\mathrm{VVmin}} = \left(1 - \delta_{\mathrm{V}}\right) G_{\mathrm{VVN}}. \end{cases} \tag{14}$$

The values of the mutual inductance M_{P1S1} versus misalignment are larger than zero, so the relationship between G_{VV} and M_{P1S1} is illustrated in Fig. 5, which mainly includes three types of voltage gain profile. The voltage gain increases with the mutual inductance M_{P1S1} first and decreases with it later. When the mutual inductance is equal to M_{P1S1D}, the voltage gain can reach the maximum value. It can be derived by setting the derivative of G_{VV} to 0, namely

$$\frac{dG_{\mathrm{VV}}\left(M_{\mathrm{P1S1}}\right)}{dM_{\mathrm{P1S1}}} = 0. \tag{15}$$

After solving (15), it gives

$$M_{\mathrm{P1S1D}} = \sqrt{\frac{L_1 L_2}{a}}. \tag{16}$$

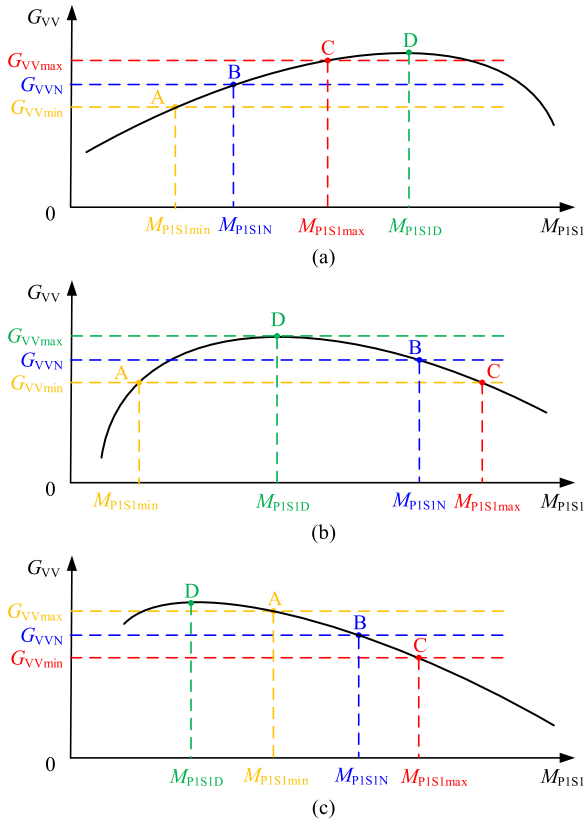

Fig. 5. Relationship between G_{VV} and M_{P1S1}. (a) $M_{\mathrm{P1S1max}} \leq M_{\mathrm{P1S1N}}$. (b) $M_{\mathrm{P1S1min}} < M_{\mathrm{P1S1N}} < M_{\mathrm{P1S1max}}$. (c) $M_{\mathrm{P1S1N}} \leq M_{\mathrm{P1S1min}}$.

With the same output voltage fluctuation in different situations, it is better to obtain the larger mutual inductance variation range (i.e., larger misalignment distance) for the IPT system. The mutual inductance variation range VR_M is defined as the difference of M_{P1S1min} and M_{P1S1max} (i.e., $VR_M = M_{\mathrm{P1S1max}} - M_{\mathrm{P1S1min}}$). Therefore, the largest VR_M should be selected among the three types (see Fig. 5). The discussions about these types are listed in Table I. Then, the values of VR_{Ma}, VR_{Mb}, and VR_{Mc} should be compared and the largest one should be selected. The difference of VR_{Mc} and VR_{Ma} is given by

$$d\_VR_{ca} = VR_{\mathrm{Mc}} - VR_{\mathrm{Ma}} = \frac{L_2\left(G_{\mathrm{VVmax}} - G_{\mathrm{VVmin}}\right)}{aG_{\mathrm{VVmax}}G_{\mathrm{VVmin}}}. \tag{17}$$

Since $L_2 > 0$, $G_{\mathrm{VVmax}} > G_{\mathrm{VVmin}} > 0$, and $a > 0$. The value of d_VR_{ca} is larger than zero, namely, VR_{Mc} is larger than VR_{Ma}. Similarly, we can find VR_{Mb} is larger than VR_{Mc}. Therefore, the mutual inductance variation range of Fig. 5(b) is the largest one, i.e.

$$\max\left\{VR_{\mathrm{Ma}},\ VR_{\mathrm{Mb}},\ VR_{\mathrm{Mc}}\right\} = VR_{\mathrm{Mb}} \tag{18}$$

where "max{ ...}" means returning the largest of two or more values.

TABLE I
THREE TYPES OF VOLTAGE GAIN PROFILE

Types	Fig. 5(a)	Fig. 5(b)	Fig. 5(c)
Constraint condition	$G_{VV}(M_{P1S1min}) = G_{VVmin}$ $G_{VV}(M_{P1S1max}) = G_{VVmax}$ $M_{P1S1min} < M_{P1S1N} < M_{P1S1max} < M_{P1S1D}$	$G_{VV}(M_{P1S1min}) = G_{VVmin}$ $G_{VV}(M_{P1S1max}) = G_{VVmin}$ $M_{P1S1min} < M_{P1S1D} < M_{P1S1N} < M_{P1S1max}$	$G_{VV}(M_{P1S1min}) = G_{VVmax}$ $G_{VV}(M_{P1S1max}) = G_{VVmin}$ $M_{P1S1D} < M_{P1S1min} < M_{P1S1N} < M_{P1S1max}$
VR_M	$VR_{Ma} = \frac{\sqrt{(bG_{VVmax}-L_2)^2-4aL_1L_2G_{VVmax}^2}+L_2}{2aG_{VVmax}} + \frac{\sqrt{(bG_{VVmin}-L_2)^2-4aL_1L_2G_{VVmin}^2}-L_2}{2aG_{VVmin}}$	$VR_{Mb} = \frac{\sqrt{(bG_{VVmin}-L_2)^2-4aL_1L_2G_{VVmin}^2}}{aG_{VVmin}}$	$VR_{Mc} = \frac{\sqrt{(bG_{VVmin}-L_2)^2-4aL_1L_2G_{VVmin}^2}+L_2}{2aG_{VVmin}} - \frac{\sqrt{(bG_{VVmax}-L_2)^2-4aL_1L_2G_{VVmax}^2}+L_2}{2aG_{VVmax}}$

TABLE II
SYSTEM SPECIFICATION AND PARAMETER VALUES

Parameter	value	Parameter	value
V_{in}	300 V	V_o	240 V
f	85 kHz	L_1	38.74 μH
C_1	90.50 nF	C_{P1}	18.82 nF
C_{P2}	16.40 nF	C_e	20.03 nF
L_{P1}	225.06 μH	L_{P2}	213.80 μH
L_{S1}	223.14 μH	L_{S2}	209.88 μH
M_{P1S1}	50.34 μH	M_{P2S2}	20.98 μH
C_{S1}	15.71 nF	C_{S2}	21.01 nF
C_2	84.46 nF	L_2	43.04 μH
a	1.07	b	-33.44×10^{-6}
δ_V	5%	EGC	1.25

In Fig. 5(b), when the air gap decreases from the NOP (i.e., the mutual inductance increases), the voltage gain will drop from B to C. When the air gap or x-/y-misalignment increase from the NOP (i.e., the mutual inductance decrease), the voltage gain will rise from B to D (maximum value) and then drops to A. Substituting point B (M_{P1S1N}, G_{VVN}) and D (M_{P1S1D}, G_{VVmax}) into (13), we can get

$$\begin{cases} \left(\frac{aM_{P1S1N}+b}{L_2}+\frac{L_1}{M_{P1S1N}}\right)^{-1} = G_{VVN} \\ \left(\frac{aM_{P1S1D}+b}{L_2}+\frac{L_1}{M_{P1S1D}}\right)^{-1} = G_{VVmax}. \end{cases} \tag{19}$$

After solving (19), L_1 and L_2 are obtained as

$$\begin{cases} L_1 = \frac{M_{P1S1N}\left[BG_{VVmax}+M_{P1S1N}\left(A-aM_{P1S1N}G_{VVmax}^2\right)\right]}{G_{VVN}G_{VVmax}\left(B-bG_{VVN}M_{P1S1N}-2aG_{VVmax}M_{P1S1N}^2\right)} \\ L_2 = \frac{G_{VVmax}\left(bG_{VVN}M_{P1S1N}-B+2aG_{VVmax}M_{P1S1N}^2\right)}{G_{VVN}M_{P1S1N}} \end{cases} \tag{20}$$

where

$$\begin{cases} A = (G_{VVN}-G_{VVmax})\left(bG_{VVN}+G_{VVN}M_{P1S1N} \right. \\ \qquad \left. + aG_{VVmax}M_{P1S1N}\right) \\ B = 2\sqrt{-aAM_{P1S1N}^3}. \end{cases} \tag{21}$$

As a result, the parameters of the hybrid IPT system can be derived according to (1), (3), and (20). The theoretically designed parameters of a setup system at the NOP (0, 0, 150) are listed in Table II.

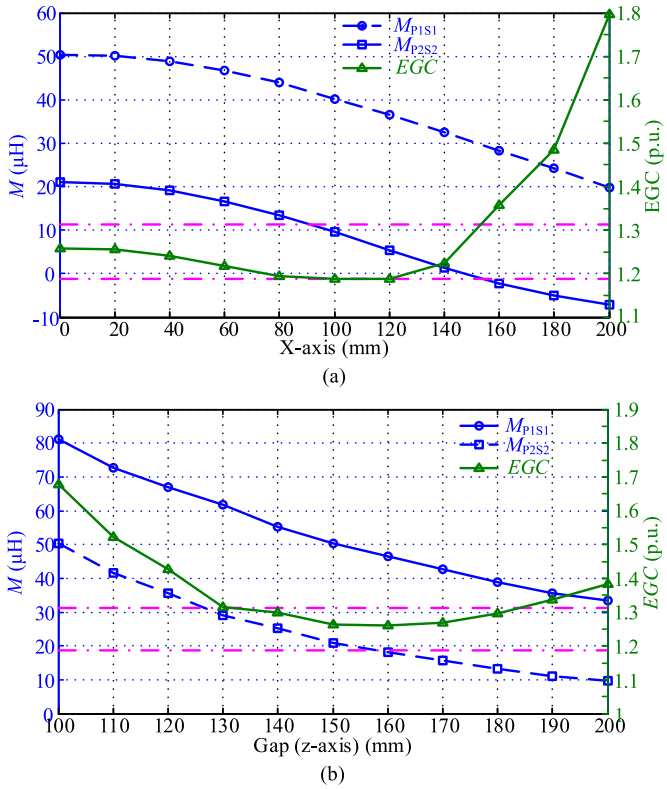

Fig. 6. EGC versus misalignment in the (a) x-direction and (b) z-direction.

The EGC with misalignment in the x- and z-directions is drawn in Fig. 6. It indicates that the maximum x-misalignment can be 150 mm if the variation of the EGC is less than 5%. Likewise, the air gap can change between 130 and 185 mm if the variation of the EGC is within 5%. In other words, with the designed parameters for the hybrid IPT system, the output voltage fluctuation is limited to 5% while the system tolerates −150–+ 150 mm x/y-misalignment and −20–+ 35 mm z-misalignment, respectively.

C. Series-Hybrid System Versus Parallel-Hybrid System

Some comparisons between the hybrid systems proposed in this article and in [29] are made in terms of operating range, efficiency, cost, complexity, etc. For simplification in presentation, the proposed hybrid system in this article is labeled as

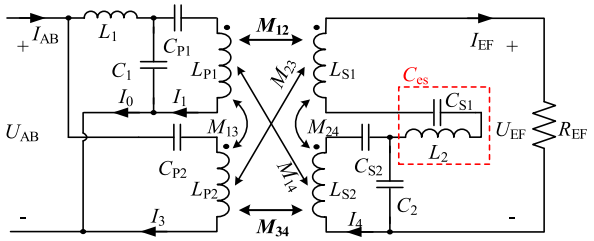

Fig. 7. Parallel-hybrid system in [29].

TABLE III
COMPARISON BETWEEN THE SERIES- AND PARALLEL-HYBRID SYSTEMS

Comparative item	Series-hybrid system	Parallel-hybrid system
Number of coils	2 QDPs+2 QPs	2 DDPs+2 QPs
Number of inductors	1	1
Number of capacitors	6	6
Cost	high	high
Complexity	high	high
Output characteristic	constant voltage	constant voltage
Peak efficiency	94.0%	93.9%
Topology structure	Input-series-output-parallel	Input-parallel-output-series
Misalignment range	x-misalignment: ±150 mm y- misalignment: ±150 mm z- misalignment: -20mm~+35 mm	x- misalignment: ±200 mm y- misalignment: ±50 mm z- misalignment: ±50 mm
Operate without pickup	Yes	No

"series-hybrid system" while that in [29] is noted as "parallel-hybrid system." Since a reconfigurable topology is used for the constant current and constant voltage charging in [29], only the parallel-hybrid topology, as shown in Fig. 7, is considered in the comparisons. The comparison results are outlined in Table III. It is evident that the cost and complexity of the two methods are both high, and the peak efficiencies are nearly close. Besides, the *y*-misalignment range in the series-hybrid system is triple as that in the parallel-hybrid system, but as a tradeoff, the *x*- and *z*-misalignment ranges in the series-hybrid system are a little bit smaller. Last but not the least, the series-hybrid system can operate safely when the pickup moves out of the operating region, while the parallel-hybrid system cannot.

For possible applications, the series-hybrid system with QDQPs is suitable for the stationary IPT charging system of EV because the *x*-, *y*-, and *z*-misalignments are considered. If the QDQPs are replaced by the double-D quadrature pads, it is suitable for the dynamic IPT charging system of EV because the *x*- and *z*-directions are predominantly considered.

IV. EXPERIMENTAL RESULTS

A. Experimental Prototype

Aiming at demonstrating the validity of the proposed method, a 3.5-kW prototype IPT system was implemented, as illustrated in Fig. 8. Detailed system parameters are listed in Table II. The coils are wound by AWG38 Litz wire. Each QP (L_{P1} or L_{S1}) has 15 turns, and each D of QDP (L_{P2} or L_{S2}) has 12 turns. The switching devices are $Q_1 - Q_4 =$ C2M0080120D and $D_1 - D_4 =$ DSEI 2 × 61-06C. A dc source is utilized on the primary side and an electronic load is used to test the output voltage of the proposed hybrid IPT system on the secondary side. The system uses an open-loop controller for the inverter to show the ability of the hybrid system tolerating pad misalignment.

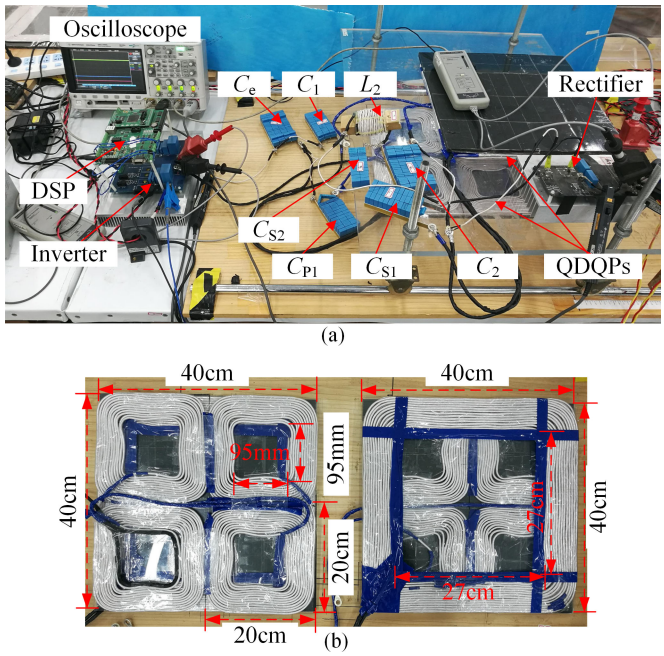

Fig. 8. (a) Setup of the hybrid IPT system. (b) Coil structure.

B. Experimental Results

When the primary and secondary sides are well aligned, the input and output dc voltages are 300 and 240 V, as shown in Fig. 9. It is evident that there is nearly no phase angle between the output current and voltage of the inverter, which means ZPA is realized and it is coincident with the theoretical analysis. Fig. 9(b) indicates that the output power is 3.58 kW with a dc–dc efficiency of 93.96%.

Fig. 10 shows the experimental waveforms of the system with +150 mm *x*-misalignment and +35 mm *z*-misalignment. It demonstrates that ZPA can still be achieved so that the system can operate with relatively high efficiency.

With the *x*- and *z*-misalignment, the output voltage and efficiency are drawn in Fig. 11(a) and (b). It should be noted that a similar output voltage profile is observed with *y*-misalignment. Since the longitudinal misalignment performances are similar to those of the lateral misalignment, the results are not presented again. The output voltage first increases and then decreases within the predetermined misalignment range. The system efficiency drops along the *x*-misalignment, while it rises when the air gap decreases and drops when the gap increases. The

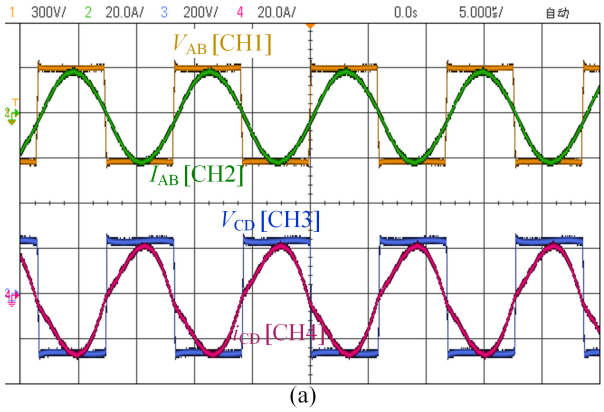

(a)

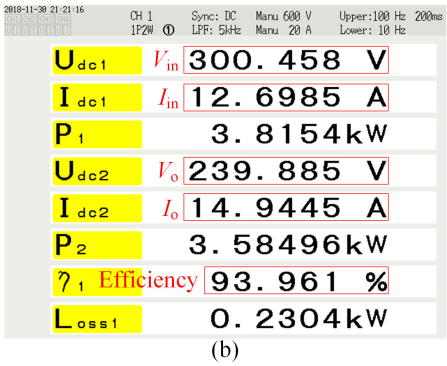

(b)

Fig. 9. Experimental waveforms of v_{AB}, i_{AB}, v_{CD}, and i_{CD} in the (a) well-aligned case and (b) corresponding efficiency.

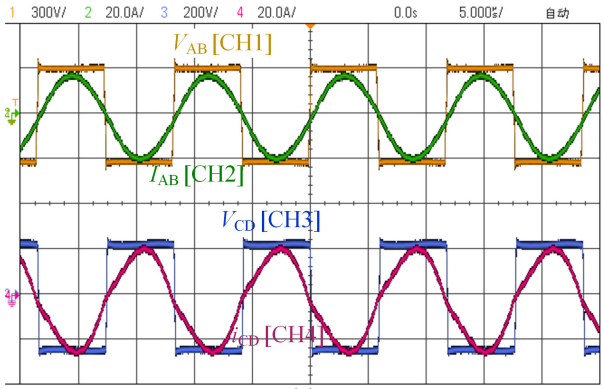

(a)

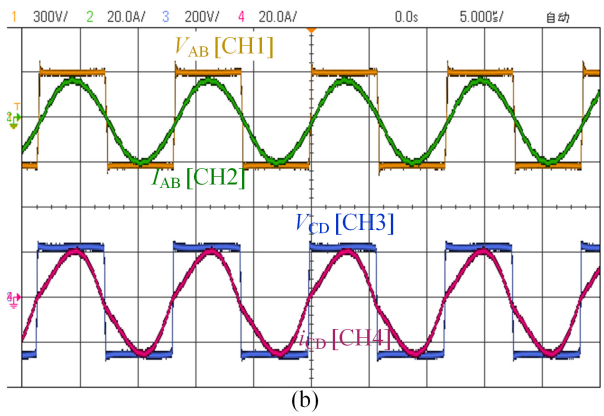

(b)

Fig. 10. Experimental waveforms of v_{AB}, i_{AB}, v_{CD}, and i_{CD}. (a) In +150 mm x-misalignment case. (b) In +35 mm z-misalignment case.

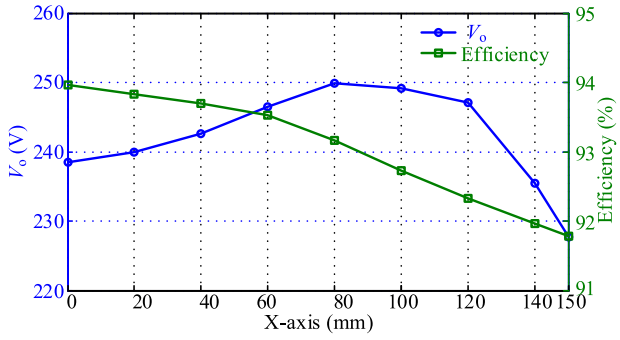

(a)

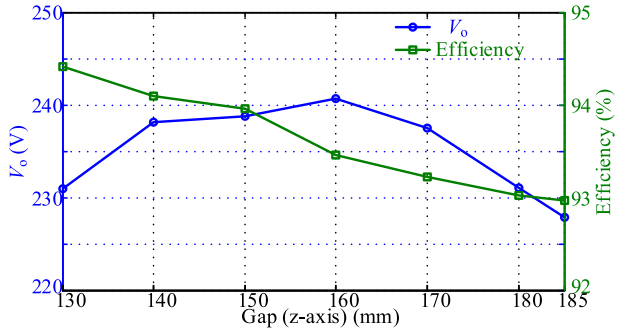

(b)

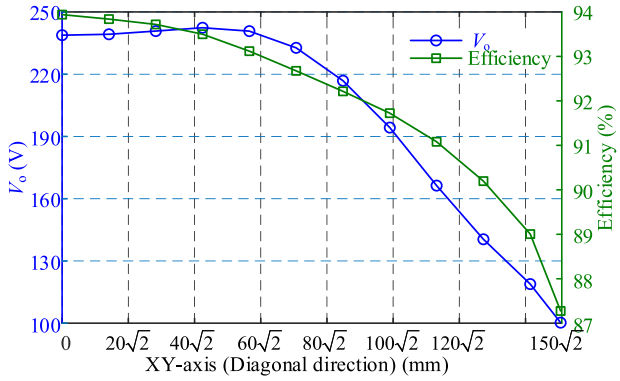

(c)

Fig. 11. Output voltage and efficiency of the hybrid IPT system with (a) x-misalignment, (b) z-misalignment, and (c) diagonal misalignment.

output voltage variation δ_V is always less than 5% with the predetermined misalignment range, which is in accordance with the analysis. It validates that the proposed hybrid system has good misalignment performance. Fig. 11(c) depicts the output voltage and efficiency of the hybrid system with diagonal misalignment. The output voltage fluctuation is larger than 5% when the diagonal misalignment exceeds 100 mm due to the cross couplings (M_{P1S2} and M_{P2S1}).

As shown in Fig. 12, the resistance of the electronic load changes from 16 to 32 Ω and then back to 16 Ω in +35 mm z-misalignment case. The output voltage changes from 228.1 to 234.5 V and back to 228.1 V. With 100% load change, the output voltage regulation is only 2.8%, mainly due to the resonant component parameter deviations. However, compared with the change of the load, the variation of the output voltage is quite small. Therefore, the output voltage of the system can

TABLE IV
COMPARISON WITH OTHER METHODS

Comparison items	Maximum pad size (cm)	Gap (cm)	Misalignment range (cm) (Misalignment percentage)	Load-independent output	Output fluctuation	Limitation of the primary current
[11]	73.8×39.1	12	x-misalignment: -8 ~ +12 (16.3%) y-misalignment: ±16 (40.9%) z-misalignment: ±2 (16.7%)	Constant current	5%	Yes
[12]	90×110	15	x-misalignment: ±20 (22.2%) y-misalignment: ±40 (36.4%) z-misalignment: ±5 (33.3%)	Constant current	29%	No
[19]	Diameter = 20	1	x-misalignment: ±5 (25%) y-misalignment: ±5 (25%) z-misalignment: -0.4 ~ +1 (100%)	Constant current	31%	No
[22]	40×40	N/A	x-misalignment: ±17.7 (44.3%) y-misalignment: ±17.7 (44.3%) z-misalignment: N/A	No	22.2%	Yes
[23]	Diameter = 32.6	10	x -misalignment: ±10 (30.7%) y-misalignment: ±10 (30.7%) z-misalignment: N/A	No	20%	Yes
[24]	45×45	12	x-misalignment: ±15 (33.3%) y-misalignment: ±15 (33.3%) z-misalignment: N/A	No	43.2%	Yes
[26]	Diameter = 9.6	3.5	x-misalignment: ±4 (41.7%) y-misalignment: ±4 (41.7%) z-misalignment: ±1	No	20%	Yes
[27]	40×80	15	x-misalignment: ±12 (30%) y-misalignment: ±12 (15%) z-misalignment: N/A	No	25%	Yes
[28]	39.1×73.8	12	x-misalignment: ±15 (38.4%) y-misalignment: ±15 (20.3%) z-misalignment: -2 ~ +2 (16.7%)	Constant current	10%	No
This work	40×40	15	x-misalignment: ±15 (37.5%) y-misalignment: ±15 (37.5%) z-misalignment: -2 ~ +3.5 (23.3%)	Constant voltage	5%	Yes

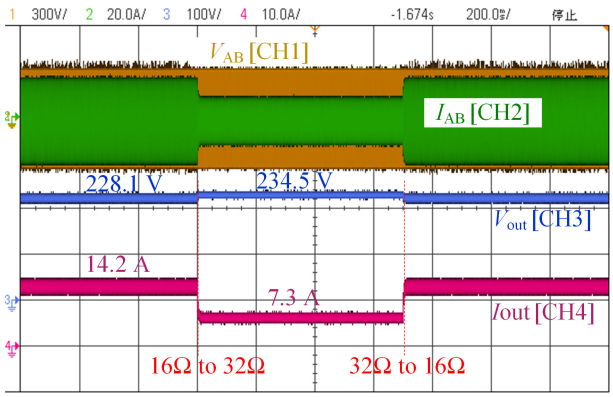

Fig. 12. Experimental waveforms when sudden load change happens with +35 mm z-misalignment.

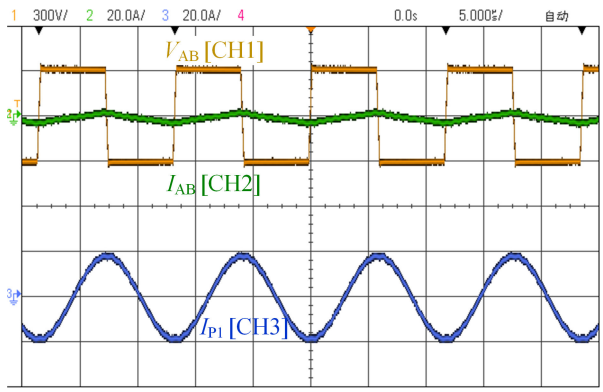

Fig. 13. Experimental waveforms of v_{AB}, i_{AB}, and i_{P1} when the pickup moves far away from the primary side.

be regarded as load independent. In the x-, y-, and diagonal-misalignment cases, the system also holds this characteristic.

Fig. 13 illustrates the waveforms of the output current and voltage of the inverter and current in the primary coil when the secondary side moves out of the operating region (M_{P1S1} and M_{P2S2} are close to 0). The current I_{AB} decrease is caused by the increase in input impedance when the distance between the pads increases. It is evident that the proposed hybrid IPT system can work safely when the pickup moves far away from the primary side. The primary coil current can generate a large magnetic field affecting the surrounded environment. In this circumstance, the high-frequency inverter should be shut down to reduce the magnetic field.

C. Comparison With Other Methods

In order to show the superiority of the proposed hybrid topology, the performance of the proposed method has been compared with the other methods, as given in Table IV. Compared with the methods [22]–[27], the proposed method has a much smaller output fluctuation, and the output is load independent. Compared with methods [12], [19], [28], the proposed topology has a lower output variation, and it can limit the primary inverter current

when the receiver moves out of the operating region. Compared with the method [11], the proposed approach has a little bit smaller *y*-misalignment range, but larger *x*- and *z*-misalignment ranges.

V. Conclusion

In this article, a hybrid IPT system using QDQPs is proposed to improve the misalignment performance. The hybrid system is formed by *LCC*-S and S-*LCC* compensation topologies. When the pickup moves out of the operating region, the primary side degrades to *LCC* compensation topology, which can avoid the drawback of the traditional primary S compensation topology. The proposed approach can tolerate misalignment in the *x*, *y*, *z*, and diagonal directions with a load-independent output voltage. On the basis of the misalignment characteristic of the QDQPs, an innovative parametric design method is given to limit the output voltage variation within a certain range. To verify the theoretical analysis, a 3.5-kW prototype with the proposed approach was built. The output voltage fluctuation of the system is within 5% when the secondary side is misaligned from -150 to $+150$ mm along the *x*-/*y*-axis, -20 to $+35$ mm along the *z*-axis, and -100 to $+100$ mm along the diagonal direction. The experimental results demonstrate good misalignment performance of the proposed hybrid IPT system. Moreover, the functionality of load-independent output voltage and the primary-side current restriction have also been successfully tested and verified in the experiment.

References

[1] S. Y. Hui, "Planar wireless charging technology for portable electronic products and Qi," *Proc. IEEE*, vol. 101, no. 6, pp. 1290–1301, Jun. 2013.

[2] A. K. RamRakhyani, S. Mirabbasi, and M. Chiao, "Design and optimization of resonance-based efficient wireless power delivery systems for biomedical implants," *IEEE Trans. Biomed. Circuits Syst.*, vol. 5, no. 1, pp. 48–63, Feb. 2011.

[3] H. Fukuda, N. Kobayashi, K. Shizuno, S. Yoshida, M. Tanomura, and Y. Hama, "New concept of an electromagnetic usage for contactless communication and power transmission in the ocean," in *Proc. IEEE Int. Underwater Technol. Symp.*, Tokyo, Japan, 2013, pp. 1–4.

[4] W. Y. Lee *et al.*, "Finite-width magnetic mirror models of mono and dual coils for wireless electric vehicles," *IEEE Trans. Power Electron.*, vol. 28, no. 3, pp. 1413–1428, Mar. 2013.

[5] D. H. Tran, V. B. Vu, and W. Choi, "Design of a high-efficiency wireless power transfer system with intermediate coils for the on-board chargers of electric vehicles," *IEEE Trans. Power Electron.*, vol. 33, no. 1, pp. 175–187, Jan. 2018.

[6] Z. Li, C. Zhu, J. Jiang, K. Song, and G. Wei, "A 3-kW wireless power transfer system for sightseeing car supercapacitor charge," *IEEE Trans. Power Electron.*, vol. 32, no. 5, pp. 3301–3316, May 2017.

[7] H. H. Wu, A. Gilchrist, K. D. Sealy, and D. Bronson, "A high efficiency 5 kW inductive charger for EVs using dual side control," *IEEE Trans. Ind. Inform.*, vol. 8, no. 3, pp. 585–595, Aug. 2012.

[8] A. Berger, M. Agostinelli, S. Vesti, J. Oliver, J. A. Cobos, and M. Huemer, "A wireless charging system applying phase-shift and amplitude control to maximize efficiency and extractable power," *IEEE Trans. Power Electron.*, vol. 30, no. 11, pp. 6338–6348, Nov. 2015.

[9] C. Xia, W. Wang, S. Ren, X. Wu, and Y. Sun, "Robust control for inductively coupled power transfer systems with coil misalignment," *IEEE Trans. Power Electron.*, vol. 33, no. 9, pp. 8110–8122, Sep. 2018.

[10] A. P. Sample, D. T. Meyer, and J. R. Smith, "Analysis, experimental results, and range adaptation of magnetically coupled resonators for wireless power transfer," *IEEE Trans. Ind. Electron.*, vol. 58, no. 2, pp. 544–554, Feb. 2011.

[11] L. Zhao, D. J. Thrimawithana, U. K. Madawala, A. P. Hu, and C. C. Mi, "A misalignment-tolerant series-hybrid wireless EV charging system with integrated magnetics," *IEEE Trans. Power Electron.*, vol. 34, no. 2, pp. 1276–1285, Feb. 2019.

[12] S. Y. Choi, J. Huh, W. Y. Lee, and C. T. Rim, "Asymmetric coil sets for wireless stationary EV chargers with large lateral tolerance by dominant field analysis," *IEEE Trans. Power Electron.*, vol. 29, no. 12, pp. 6406–6420, Dec. 2014.

[13] G. A. J. Elliott, S. Raabe, G. A. Covic, and J. T. Boys, "Multiphase pickups for large lateral tolerance contactless power-transfer systems," *IEEE Trans. Ind. Electron.*, vol. 57, no. 5, pp. 1590–1598, May 2010.

[14] X. Liu and S. Y. Hui, "Optimal design of a hybrid winding structure for planar contactless battery charging platform," *IEEE Trans. Power Electron.*, vol. 23, no. 1, pp. 455–463, Jan. 2008.

[15] Z. Zhang and K. T. Chau, "Homogeneous wireless power transfer for move-and-charge," *IEEE Trans. Power Electron.*, vol. 30, no. 11, pp. 6213–6220, Nov. 2015.

[16] M. Budhia, J. T. Boys, G. A. Covic, and C.-Y. Huang, "Development of a single-sided flux magnetic coupler for electric vehicle IPT charging systems," *IEEE Trans. Ind. Electron.*, vol. 60, no. 1, pp. 318–328, Jan. 2013.

[17] A. Zaheer, H. Hao, G. A. Covic, and D. Kacprzak, "Investigation of multiple decoupled coil primary pad topologies in lumped IPT systems for interoperable electric vehicle charging," *IEEE Trans. Power Electron.*, vol. 30, no. 4, pp. 1937–1955, Apr. 2015.

[18] S. Kim, G. A. Covic, and J. T. Boys, "Tripolar pad for inductive power transfer systems for EV charging," *IEEE Trans. Power Electron.*, vol. 32, no. 7, pp. 5045–5057, Jul. 2017.

[19] C. Zheng, H. Ma, J.-S. Lai, and L. Zhang, "Design considerations to reduce gap variation and misalignment effects for the inductive power transfer system," *IEEE Trans. Power Electron.*, vol. 30, no. 11, pp. 6108–6119, Nov. 2015.

[20] X. Dai, L. Li, X. Yu, Y. Li, and Y. Sun, "A novel multi-degree freedom power pickup mechanism for inductively coupled power transfer system," *IEEE Trans. Magn.*, vol. 53, no. 5, May 2017, Art no. 8600107.

[21] D. Lin, C. Zhang, and S. Y. R. Hui, "Mathematic analysis of omnidirectional wireless power transfer—Part-II: Three-dimensional systems," *IEEE Trans. Power Electron.*, vol. 32, no. 1, pp. 613–624, Jan. 2017.

[22] Q. Zhu, Y. Guo, L. Wang, C. Liao, and F. Li, "Improving the misalignment tolerance of wireless charging system by optimizing the compensate capacitor," *IEEE Trans. Ind. Electron.*, vol. 62, no. 8, pp. 4832–4836, Aug. 2015.

[23] H. Feng, T. Cai, S. Duan, J. Zhao, X. Zhang, and C. Chen, "An LCC-compensated resonant converter optimized for robust reaction to large coupling variation in dynamic wireless power transfer," *IEEE Trans. Ind. Electron.*, vol. 63, no. 10, pp. 6591–6601, Oct. 2016.

[24] F. Lu, H. Zhang, H. Hofmann, W. Su, and C. C. Mi, "A dual-coupled LCC-compensated IPT system with a compact magnetic coupler," *IEEE Trans. Power Electron.*, vol. 33, no. 7, pp. 6391–6402, Jul. 2018.

[25] J. Zhao, T. Cai, S. Duan, H. Feng, C. Chen, and X. Zhang, "A general design method of primary compensation network for dynamic WPT system maintaining stable transmission power," *IEEE Trans. Power Electron.*, vol. 31, no. 12, pp. 8343–8358, Dec. 2016.

[26] H. Feng, T. Cai, S. Duan, X. Zhang, H. Hu, and J. Niu, "A dual-side-detuned series–series compensated resonant converter for wide charging region in a wireless power transfer system," *IEEE Trans. Ind. Electron.*, vol. 65, no. 3, pp. 2177–2188, Mar. 2018.

[27] J. L. Villa, J. Sallan, J. F. S. Osorio, and A. Llombart, "High-misalignment tolerant compensation topology for ICPT systems," *IEEE Trans. Ind. Electron.*, vol. 59, no. 2, pp. 945–951, Feb. 2012.

[28] L. Zhao, D. J. Thrimawithana, and U. K. Madawala, "Hybrid bidirectional wireless EV charging system tolerant to pad misalignment," *IEEE Trans. Ind. Electron.*, vol. 64, no. 9, pp. 7079–7086, Sep. 2017.

[29] Y. Chen, B. Yang, Z. Kou, Z. He, G. Cao, and R. Mai, "Hybrid and reconfigurable IPT systems with high-misalignment tolerance for constant current and constant voltage battery charging," *IEEE Trans. Power Electron.*, vol. 33, no. 10, pp. 8259–8269, Oct. 2018.

[30] Y. Chen *et al.*, "Variable-parameter T-circuit based IPT system charging battery with constant current or constant voltage output," *IEEE Trans. Power Electron.*, vol. 35, no. 2, pp. 1672–1684, Feb. 2020.

[31] S. Ahn *et al.*, "Reduction of electromagnetic field (EMF) of wireless power transfer system using quadruple coil for laptop applications," in *Proc. IEEE MTT-S Int. Microw. Workshop Ser. Innov. Wireless Power Transmiss., Technol., Syst., Appl.*, Kyoto, Japan, 2012, pp. 65–68.

[32] A. Ahmad, M. S. Alam, and A. A. S. Mohamed, "Design and interoperability analysis of quadruple pad structure for electric vehicle wireless charging application," *IEEE Trans. Transp. Electrific.*, to be published.
[33] R. W. Erickson and D. Maksimovic, *Fundamentals of Power Electronics*, 2nd ed. Norwell, MA, USA: Kluwer, 2001.
[34] Y. Yao, Y. Wang, X. Liu, K. Lu, and D. Xu, "Analysis and design of an S/SP compensated IPT system to minimize output voltage fluctuation versus coupling coefficient and load variation," *IEEE Trans. Veh. Technol.*, vol. 67, no. 10, pp. 9262–9272, Oct. 2018.

Yang Chen (S'17) received the B.Sc. degree in electrical engineering and automation in 2015 from Southwest Jiaotong University, Chengdu, China, where he is currently working toward the Ph.D. degree in electrical engineering. He is also working toward a joint Ph.D. degree with Future Energy Electronics Center, Virginia Tech, Blacksburg, VA, USA.

In 2018, he received the State Scholarship Fund of China Scholarship Council. His research interests include wireless power transfer, especially on compensation topology and misalignment tolerance improvement.

Bin Yang received the B.Sc. degree in electrical engineering and automation from East China Jiaotong University, Nanchang, China, in 2017. He is currently working toward the M.Sc. degree in electrical engineering with the School of Electrical Engineering, Southwest Jiaotong University, Chengdu, China.

His main research interest is wireless power transfer.

Xiaobing Zhou received the B.Sc. degree in electrical engineering and automation from East China Jiaotong University, Nanchang, China, in 2017. He is currently working toward the M.Sc. degree in electrical engineering with the School of Electrical Engineering, Southwest Jiaotong University, Chengdu, China.

His main research interest is wireless power transfer.

Qiao Li received the B.Sc. degree in electrical engineering and automation from the Chengdu University of Technology, Chengdu, China, in 2017. He is currently working toward the M.Sc. degree in electrical engineering with the School of Electrical Engineering, Southwest Jiaotong University, Chengdu, China.

His main research interest is wireless power transfer.

Zhengyou He (M'10–SM'13) received the B.Sc. and M.Sc. degrees in computational mechanics from Chongqing University, Chongqing, China, in 1992 and 1995, respectively, and the Ph.D. degree in power system and automation from Southwest Jiaotong University, Chengdu, China, in 2001.

He is currently a Professor with the School of Electrical Engineering, Southwest Jiaotong University. His research interests include signal process and information theory applied to the electrical power system and application of wavelet transforms in power system.

Ruikun Mai (M'14) received the B.Sc. degree in electronic and information engineering and the Ph.D. degree in power system and automation from Southwest Jiaotong University, Chengdu, China, in 2004 and 2010, respectively.

He is currently a Professor with the School of Electrical Engineering, Southwest Jiaotong University, Chengdu, China. His research interests include wireless power transfer and its application in railway systems, and power system stability and control.

Jih-Sheng Lai (S'85–M'89–SM'93–F'07–LF'19) received the M.S. and Ph.D. degrees in electrical engineering from the University of Tennessee, Knoxville, TN, USA, in 1985 and 1989, respectively.

In 1989, he joined the Electric Power Research Institute (EPRI) Power Electronics Applications Center, where he managed EPRI-sponsored power electronics research projects. In 1993, he then joined as a Power Electronics Lead Scientist with the Oak Ridge National Laboratory, where he initiated a high-power electronics program and developed several novel high-power converters including multilevel converters and soft-switching inverters. In 1996, he joined Virginia Polytechnic Institute and State University. He is currently the James S. Tucker Professor with the Department of Electrical and Computer Engineering and the Director of Future Energy Electronics Center. He has authored or coauthored more than 450 refereed technical papers, one book chapter, two books, and 27 patents. His main research areas include high-efficiency power electronics conversions for high power and energy applications.

Dr. Lai was a recipient of the Technical Achievement Award in Lockheed Martin Award Night, two Journal Paper Awards, 12 Best Paper Awards from the IEEE sponsored conferences, and 2016 IEEE IAS Gerald Kliman Innovator Award. He led the student teams to win the Top Three Finalist in Google Little Box Challenge in 2016, Grand Prize Award from International Future Energy Challenge in 2011, and Grand Prize Award from Texas Instruments Engibous Analog Design Competition in 2009. He is the Founding Chairs of 2001 IEEE IFEC and 2016 IEEE ACEPT, General Chairs of IEEE COMPEL-2000, IEEE APEC 2005, IEEE SPEC-2018, and IEEE IFEEC-2019 conferences.